Proceedings of ASME Turbo Expo 2016: Turbomachinery Technical Conference and Exposition
GT2016
June 13 – 17, 2016, Seoul, South Korea

GT2016-58098

PRESSURE DISTORTION EFFECTS ON RIM SEAL PERFORMANCE IN A LINEAR CASCADE

Jeffrey Gibson
The Pennsylvania State University
State College, PA, USA*

Karen Thole
The Pennsylvania State University
State College, PA, USA

Jesse Christophel
Pratt & Whitney
East Hartford, CT, USA

Curtis Memory
Pratt & Whitney
East Hartford, CT, USA

Thomas Praisner
Pratt & Whitney
East Hartford, CT, USA

ABSTRACT

Rim seals are used to prevent the ingress of hot gas into the cavities beneath turbine platforms. As these cavities are not actively cooled, high-pressure air, known as purge flow, is taken from the compressor and introduced beneath the platform to prevent hot gas from penetrating through the gaps between stationary and rotating hardware. Improving the rim-seal geometry however, is made difficult by a lack of understanding of the salient fluid mechanics associated with this region. This study investigates both the impact of a vane-induced static pressure distortion as well as the influence of the pressure distortion of a downstream blade row on an engine-relevant rim seal in a stationary, linear cascade. Vane alterations resulted in minimal change to rim seal performance; however, adding the pressure distortion of a downstream blade row was found to disturb the trench flow resulting in poorer performance of the seal.

INTRODUCTION

Turbine inlet temperatures are rising to meet ever more demanding engine performance requirements. Such extreme temperatures well surpass the melting temperature of turbine component materials and therefore endanger uncooled hardware. Ingress of hot gas from the main gas path into the uncooled cavities beneath turbine platforms can risk the structural integrity of the disks. In a typical application, high-pressure air from the compressor, which circumvents the combustor, is introduced into the under-platform cavities to prevent hot gas ingress and keep metal temperatures manageable. This flow will be referred to as purge flow. To reduce the amount of purge flow required to prevent ingress, a geometric feature known as a rim seal is placed below the platform between static and rotating airfoil rows. The rim seal reduces purge-flow requirements by creating a complicated flow path that discourages hot gas ingress.

Effective rim seal geometries are desirable to minimize the amount of purge flow required to prevent hot gas ingress beneath the platform and to minimize aerodynamic stage losses. Minimizing purge requirements is made difficult due to the highly unsteady and complex flowfield that exists in the region in and around the rim seal. Many factors contribute to the complexity in the flowfield in the rim seal such as rotational effects, the high tangential velocity in the rim seal area resulting from the main gas path flow being turned by the vane, as well as main gas path pressure effects. In addition to these flow features, the potential field, as well as the endwall flows of nearby airfoils, disturb the flowfield at the seal exit.

The geometry of a rim greatly influences how effective the seal is at preventing hot gas ingress and aerodynamic losses. A common seal geometry in modern gas turbines uses a series of radially overlapping geometric features to discourage ingress. An important aspect of this seal geometry is the axial distance that these features overlap, also known as the axial overlap. Increasing the axial overlap at the seal exit decreases the amount of hot gas ingress through the seal. Likewise, decreasing the width of the region where the purge flow mixes with the main gas path also improves sealing performance [1]. The impact of these geometry perturbations on the flowfield at the seal exit however is not fully described.

Presented in this paper are sealing effectiveness and adiabatic endwall effectiveness data that describe the impacts of the upstream vane, downstream bluff bodies, and seal geometry on an engine-relevant rim seal in a linear cascade. These studies were conducted in a stationary, linear cascade to isolate the effects of the pressure distortion from other complicating factors such as rotation. Three-component laser Doppler velocimetry (LDV) was used to measure the mean and turbulent flowfields to identify the mechanisms through which seal performance was affected. Flowfield measurements were taken at the exit of the seal with and without downstream bluff

*Currently at Siemens Energy

bodies present to ascertain the effect that the downstream pressure field has on the rim seal flow. Measurements were also made in a baseline seal as well as in a modified seal where the axial overlap was 332% larger than the baseline. Flowfield measurements in a stationary cascade can help inform higher-fidelity investigations that include unsteady and rotational effects.

NOMENCLATURE

C_{ax} = vane axial chord length [m]
C_B = bluff body true chord length [m]
C_p = pressure coefficient $(P - \overline{P}_{in})/\frac{1}{2}\rho_{in}\overline{U}_{in}^2$
$\dot{m}_p$ = Purge Mass Flow Rate [kg/s]
$\dot{m}_\infty$ = Main Gas Path Mass Flow Rate [kg/s]
P_v = Vane Pitch [m]
PR = Purge Rate $(\dot{m}_p/\dot{m}_\infty)$*100
s = arc length [m]
s_{max} = maximum arc length [m]
S_e = Exit Span [m]
S_i = Inlet Span [m]
T = Static Temperature [°C]
T_{aw} = Adiabatic Wall Temperature [°C]
T_∞ = Freestream Temperature [°C]
T_p = Purge Flow Temperature [°C]
TKE = Turbulent Kinetic Energy $[u^2 + v^2]/2$ $[m^2/s^2]$
Tu = Turbulence Intensity $[2TKE/3]^{1/2}/\|\vec{V}\|$
U = Mean Axial Velocity [m/s]
u = rms Axial Velocity [m/s]
U_i = Mean Inlet Velocity [m/s]
V = Mean Tangential Velocity [m/s]
v = rms Tangential Velocity [m/s]
W = Mean Radial Velocity [m/s]
w = rms Radial Velocity [m/s]
x = Axial Coordinate [m]
y = Tangential Coordinate [m]
z = Radial Coordinate [m]

Greek

θ = Momentum Boundary Layer Thickness [m]
ν = Kinematic Viscosity $[m^2/s]$
ψ = Yaw Angle $[\tan^{-1}(V/U)]$
η = Adiabatic Effectiveness $\left[(T_\infty\text{-}T_{aw})/(T_\infty\text{-}T_p)\right]$
ε = Sealing Effectiveness $\left[(T_\infty\text{-}T)/(T_\infty\text{-}T_p)\right]$

PREVIOUS STUDIES

Driving factors that cause hot gas from the mainstream to penetrate beneath the turbine platform exist in the main gas path as well as beneath the platform. Johnson et al. [2] provides an extensive summary of these factors, which include the unsteady interactions between the vane and blade pressure fields, pumping due to rotation of the disk, and turbulent transport. Phadke and Owen [3] shows that either the main gas path pressure field or disk pumping beneath the platform may dominate the ingress process depending on the axial Reynolds number in the mainstream, the rotational Reynolds number, and the seal geometry. Similarly, the pressure model of Johnson et al. [4] shows that when the vane and blade rows are closely spaced, their pressure fields interact and become a dominant influence on the ingress of hot gas beneath the platform.

In the main gas path, the pressure field of a downstream blade has a significant impact on rim seal flows. The unsteady combination of the vane and blade pressure fields can result in the simultaneous occurrence of high and low pressure regions that correspond to hot gas ingress into the seal and purge flow egress for different tangential locations in the seal [5, 6]. Green et al. [7] show that in a turbine stage rig, the presence of the upstream vane increases the pressure variation above the seal which forces hot gas beneath the endwall. The presence of a downstream blade further increases the pressure variation above the seal but results in a decrease in hot gas ingress. Bohn et al.[8] also show that the presence of a downstream blade increases the variation in pressure above the seal, but, contrary to Green et al., reports that the blade forces more hot gas into the seal. While it is unclear whether a downstream blade positively or negatively affects hot gas ingress, it is evident that both airfoils can have an impact on the flow in the rim seal.

Aside from the pressure effects, the endwall flows (horseshoe vortex) generated by a downstream blade interact with purge flow exiting the seal, as reported by Gallier et al. [9] in a one and a half-stage turbine. Depending on the blade clocking relative to the vanes, either ingress occurred or the purge flow rolled-up with the blade horseshoe vortex onto the blade surface. Alterations in the blade endwall flows due to the presence of purge flow have been extensively documented as a source for increased aerodynamic losses [10-15].

The rim seal geometry plays an important role in a seal's ability to mitigate ingress while still trying to create little aerodynamic loss. Radial overlap seals are widely used as they require much less purge flow to prevent ingress than more simple geometries like axial gap seals [16]. The overlapping geometry of radial overlap seals reduce the impact of the main gas path pressure field on the flow beneath the platform [2,4]. The benefits of a radial overlap seal are maintained as long as any overlap exists. Once the overlap is broken however, a radial overlap seal performs much like an axial gap seal, as demonstrated by Abe at al. [16]. Radial overlap seals further reduce ingress by causing the static pressure beneath the platform to increase due to purge flow impinging on the underside of the overlap [3]. Higher pressures beneath the platform cause purge flow to exit the seal rather than hot gas to enter under the platform. Increasing the overlap at the seal exit decreases hot gas ingress into the seal and increases the cooling effect of the purge flow on the downstream blade endwall [1,17].

Radial overlap seals not only require less purge flow to prevent ingress than axial gap seals but also generate lower aerodynamic losses. Radial injection of the purge flow from an axial gap seal, as shown by Paniagua et al., results in a blockage of the main gas path, altering the degree of reaction at mid-span by 11% in their case [18]. A radial overlap seal however, injects the purge flow along the endwall reducing the

mixing losses by minimizing the radial distance the purge flow penetrates the main gas path [13-15]. In linear-cascade-bladed testing, the rim seal geometry optimization work by Popovic and Hodson [19] indicated that an optimal design would use features deep in the seal such as hooks and sharp corners to limit the ingress of hot gas beneath the endwall while maintaining a smooth transition from the radial overlap to the main gas path to reduce losses. The profile of the endwall transition from the radial overlap to the blade passage affects the stage losses created by the presence of purge flow. Marini et al. show that by raising the blade endwall, the amount of viscous mixing near the endwall was reduced; leading to reduced losses [19-20].

While measurements in the literature describe the impact of a downstream blade on ingress levels, few experimental investigations are available on how the presence of a downstream blade alters the flowfield in the seal. Gallier et al. [9] gives flowfield measurements near the exit of an axial gap seal. Likewise, Roy et al. [5] measured the velocity field in the space under the turbine endwall. No measurements exist, however, to the knowledge of the authors which capture the impact of a downstream blade on the flowfield near the exit of an engine-relevant, radial overlap seal. The present work provides a detailed description of the impact of downstream bluff bodies on the flowfield at the exit of a radial overlap seal in a linear cascade. As the present work consists of data from a stationary cascade, it is anticipated that the qualitative trends observed may inform higher fidelity investigations that include unsteady and rotational effects.

EXPERIMENTAL METHODS

A stationary, linear cascade was used to make spatially-resolved measurements near the exit of an engine-relevant rim seal. The cascade was part of the large-scale, low-speed wind tunnel facility as previously described by the authors [1]. The facility employs a recirculating flow loop which was split into two streams. One stream represented the main gas path which passed through a heater bank and flow conditioning screens before reaching the test section. The other stream, representing the purge flow, was introduced into the rim seal beneath the turbine endwall through the assistance of an auxiliary blower. A turbulence intensity of 6% was set in the mainstream using a passive turbulence grid. Heating the mainstream and cooling the purge flow provided a 35° C temperature difference for ingress measurements.

The test section consisted of a linear cascade of five vanes and four flow passages, as shown in Figure 1a. A flexible wall attached to the trailing edge of the outermost vane (labeled vane 1 in Figure 1a) and a tailboard attached to the innermost vane, labeled vane 5, were used to maintain periodicity in the test section. The span of the test section decreased through the vane passage as shown in Figure 1b. Additional parameters and flow conditions for the cascade are listed in Table 1.

An important boundary condition that needed to be simulated to match that of the engine was the strong tangential velocity in the outer portions of the seal. In an actual gas turbine, the large turning angle of the vanes and the rotation of the blade induce a high tangential velocity in the region where the seal interfaces with the main gas path. An additional flow loop was included in the experiment to simulate this tangential velocity in the cascade. This cross-flow loop removed flow from the trench area of the seal beyond the tailboard of vane 5, shown in Figure 1a. The cross flow was then reintroduced to the trench at the flexible wall behind vane 1. As the cross flow created the same velocities as those in the engine, it was imperative to set the appropriate flow rate in the loop. The flow rate through the cross-flow loop was determined through both periodic CFD simulations and experimentally in the cascade. The correct flow rates provided the best agreement with CFD simulations which predicted those that best matched the conditions found in the turbine engine. Gibson et al. [1] provide further information regarding the development of the cross-flow.

Table 1. Cascade Parameters and Inlet Conditions

Number of Vanes	5
Vane Axial Chord Length (C_{ax})	0.198 m
Vane Pitch to Chord Ratio (P_v/C_{ax})	1.22
Vane Inlet Span to Chord Ratio (S_i/C_{ax})	1.91
Inlet to Exit Span Ratio (S_i/S_e)	1.21
Exit Flow Angle	72°
Inlet Reynolds Number $(U_i C_{ax}/\nu)$	63,000
Inlet Velocity (U_i)	5.85 m/s
Momentum Thickness (θ/S_i)	0.0095
Shape Factor (δ^*/θ)	1.32

The area of particular interest in the cascade was the rim seal located downstream of the vanes. The location of the rim-seal exit relative to the vanes is shown in Figure 1a. The rim-seal geometry was an engine-relevant, double-overlap seal. The area beneath the platform was modeled in these experiments as a plenum located beneath the seal from which the purge air is introduced. The purge air was removed from the top stream of the tunnel by an auxiliary blower, was cooled, and then supplied to the plenum. The flow rate of the purge air was directly measured with a laminar-flow element. The mass flow rate of the purge flow was scaled by that in the main gas path upstream of the vanes. Three different purge rates (defined as PR in the nomenclature) were included in this work: PR = 0.75%, 1.0%, and 1.5%. The purge air entered the rim seal from the plenum; traveled through the seal; and mixed with the mainstream flow in the region labeled as the trench region in Figure 1c.

Mid-span pressure distributions around the vanes were used to verify the periodicity in the main gas path. The distribution of pressure coefficient, defined as Cp in the nomenclature, for all five vanes is shown in Figure 2. Most of the vanes showed similar distributions and agreed within the stated uncertainty with periodic CFD predictions. A small difference was observed in the passage between vanes 1 and 2. No sealing effectiveness or flowfield data, however, were acquired in this

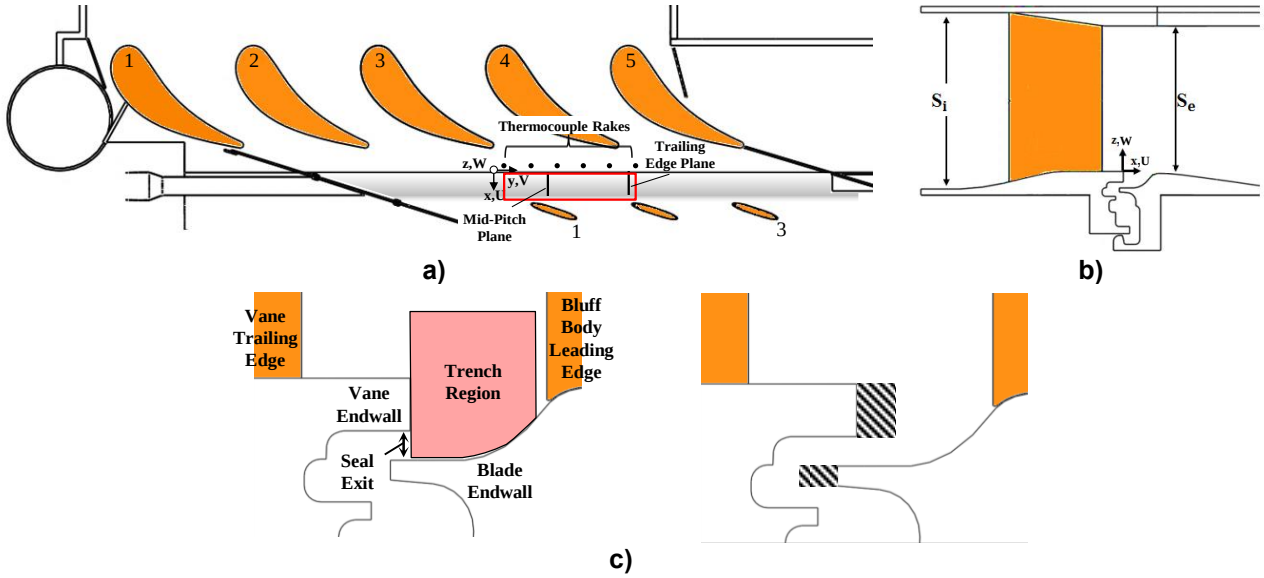

Figure 1. Description of cascade including a) top view showing the measurement locations, b) lateral view of the test section, and c) a detail of the seal exit showing the bounding surfaces.

region. Pressure taps in the vane endwall, located $0.22C_{ax}$ downstream of the vane trailing edge, were also used to verify periodicity on the vane endwall. A comparison of pressure coefficient data from the baseline seal with CFD predictions is shown in Figure 3. The uncertainty in the pressure coefficients was ascertained using the partial differential method outlined by Moffat [22]. The uncertainty was determined to be 0.4 for a low value of C_p = -17.4 and 0.03 for a high value of C_p = -1.25.

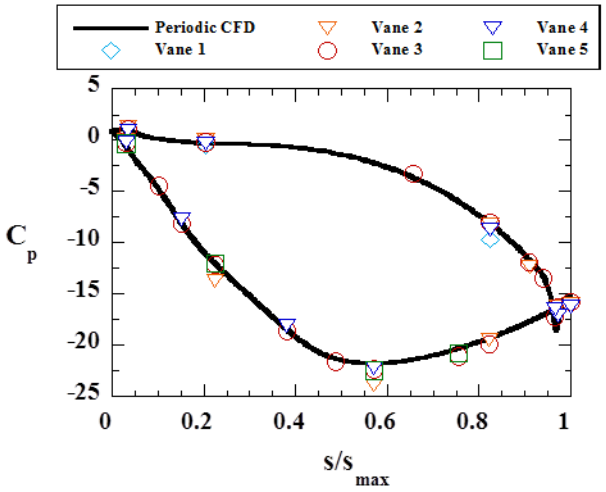

Figure 2. The static pressure distribution from the vane mid-span location.

A unique aspect of this work was the inclusion of bluff bodies that imposed a pressure boundary condition downstream of the seal similar to that of a blade, as shown in Figure 1a. The static-pressure distortion of the blade to be matched by the bluff bodies was determined from a 3D mixing-plane based steady simulation [23]. A bluff body was then designed using a two-dimensional CFD simulation to match the leading edge pressure distortion of a downstream blade at two different axial locations as discussed previously by the authors [1]. The bluff bodies were placed $0.54C_{ax}$ downstream of the vane trailing edge and angled to match the average turning angle of the vanes. All remaining geometric parameters of the bluff bodies are listed in Table 2.

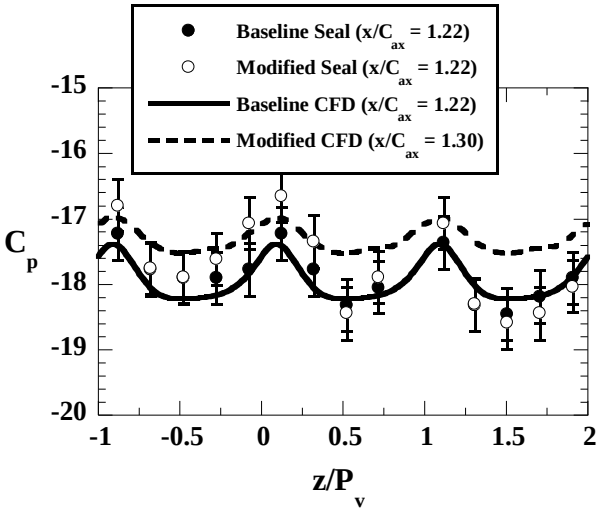

Figure 3. The static pressure distribution on the endwall from the baseline and modified seals at x/Cax =1.22 and 1.30.

Mid-span pressure distributions previously reported by the authors showed good periodicity between each of the three bluff bodies [1]. A study was also conducted to determine the effect of bluff body pitchwise locations, referred to here as

clocking, on seal performance. As part of this study, the bluff bodies were moved by a third of a their pitch in either direction from the locations shown in Figure 1a. Sealing effectiveness and adiabatic effectiveness data were taken at each clocking. Average sealing effectiveness and endwall temperatures were observed to be insensitive to different bluff body clocking positions.

Table 2. Parameters of the Bluff Bodies

Number of Bluff Bodies	3
Vane to Bluff Body Pitch Ratio P_v/P_B	1.23
Pitch to Chord Ratio P_B/C_B	2.16
Bluff Body Aspect Ratio	8
Bluff Body Angle from Axial Direction	72°

MEASUREMENT METHODOLIGIES

Two parameters were used to determine the ability of the rim seal to limit the ingress of hot gas into the seal as well as to cool the blade endwall: sealing effectiveness and adiabatic endwall effectiveness respectively. Sealing effectiveness, defined in the nomenclature as ε, was calculated from flow temperature measurements made by rakes of five thermocouples. Six rakes were evenly spaced over one vane pitch as shown in Figure 1a. Each rake spanned the seal exit as defined in Figure 1c. The measurements from all of the rakes were averaged into a single sealing effectiveness value. A sealing effectiveness value of one indicated no ingress occurring while a value of zero described a seal with high levels of ingress. The uncertainty in the calculations of sealing effectiveness was calculated using the partial differential method presented by Moffat [22]. The uncertainty in sealing effectiveness was ±0.02 for both the low values between 0.50 and 0.89.

Infrared (IR) thermography was used to measure the temperature of the adiabatic endwall just downstream of the rim seal exit. The endwall was made of expanded polystyrene with a conductivity of 0.032 W/m K. The IR images had a resolution of 2 pixels/mm and an area of 320 x 240 pixels. Images at six different locations were taken to capture the region of interest. Five separate images were taken and then averaged at each image location. These averaged images were calibrated for emissivity and reflected temperature using temperature measurements from thermocouples embedded in the endwall. From the IR measurements, adiabatic endwall effectiveness (defined as η in the nomenclature) was calculated. Similar to sealing effectiveness, an adiabatic effectiveness value of 1 corresponded to regions of high cooling by the purge flow; whereas a value of 0 corresponded to no cooling. An average adiabatic effectiveness level was calculated from the area marked by a red rectangle in Figure 1a. Uncertainty in the adiabatic effectiveness calculations was ±0.02 for both the low value of 0.22 and the high value of 0.89.

Three-component laser Doppler velocimetry (LDV) was used to measure the mean and turbulent flowfields near the seal exit. Laser beam pairs of three wavelengths were supplied by an argon-ion laser: green (514.5 nm), blue (488.0 nm), and violet (476.5 nm). A Bragg cell shifted the frequency of one beam in each pair by 40 MHz to resolve directional ambiguity. The beams passed through fiber optics to a two-component probe (green and blue) and a single component probe (violet). Each probe had a 2.6X beam expander and a 750 mm focusing lens resulting in a half-angle of 4.9° between the two beams of a pair. Backscatter mode was used on each probe where the transmitting and receiving optics were located in the same probe. The measurement volumes had a diameter/length of 72.8 µm/0.85 mm, 69.1 µm/0.81 mm, and 67.4 µm/0.79 mm for the green, blue, and violet beams respectively. Particles of di-ethyl-hexyl sebacate with a nominal diameter of 1 µm were generated with a Laskin nozzle seeder. The seed particles were introduced upstream of the tunnel fan as well as upstream of the plenum beneath the seal so the particles were evenly distributed throughout the flow.

Intersecting the measurement volumes of the three beam pairs yielded three-component, non-coincident measurements. Optical access into the trench was achieved by suspending the probes above the test section and passing the beams through a glass portion of the top endwall. The probes were angled 45° apart. It was necessary to tilt both probes by 6º, which is an angle slightly larger than the beam half-angles, to obtain measurements near the trailing edge of the vane endwall.

The flowfield measurements presented in this work focused on the region where the rim seal interfaces with the main gas path. The dimensions of the planes where the measurements were taken corresponded to the red plane in Figure 1c. Flowfield measurements were made at two pitchwise planes whose locations were marked in Figure 1a. The mid-pitch plane ($y/P= 0.6$) corresponded with a region of low pressure between vanes 3 and 4. The vane trailing edge plane ($y/P= 1.1$), however, coincided with the peak in vane endwall pressure behind vane 4 as well as the leading edge of the middle bluff body. To obtain statistically stationary data, approximately 10,000 samples were collected for each of the three measured components at each measurement location. Non-orthogonal mean velocity components were transformed into the orthogonal coordinate system of the cascade shown in Figures 1a-b. A turbulent kinetic energy (defined as TKE in the nomenclature section) was calculated from the mean rms values from the orthogonal beam pairs in the two-component probe (the green and the blue).

As determined by the perturbation method by Moffat [22], the uncertainty in the mean axial velocity, U, was 5% of 2.54 m/s. The uncertainty in mean tangential velocity was 1% of 14.37 m/s. The greatest uncertainty was for the spanwise direction since it was the nonorthogonal direction. It was calculated to be 20% of 1.5 m/s. The uncertainty in TKE was 5.4% of a high value of 17.02 m^2/s^2.

DESCRIPTION OF RIM SEAL GEOMETRY

The geometry of the rim seal, as illustrated in Figure 1c was modified to examine the impact of increasing the axial overlap

at the seal exit on the flowfield in the trench. Such increases in overlap may occur due to intentional design changes or to a lesser extent through manufacturing variability. The outline of the baseline seal as well as the extensions that constituted the modified geometry are shown in Figure 1c. For the modified geometry, the vane endwall trailing edge and the blade endwall leading edge were extended as shown by the shaded regions in Figure 1c. Each endwall was extended 166% of the length of the axial overlap in the baseline seal. As a result, the axial overlap in the modified seal was 332% longer than in the baseline. Such an extreme length was used to clearly demonstrate the impact of such a geometry length on the trench flowfield. In an engine, such modifications may lead to rubbing or increased heat transfer to the endwall much like a cooling fin. Modifying the seal increased the ratio of axial overlap to radial clearance from 0.67 in the baseline seal to 2.89 in the modified seal.

Extending the vane endwall resulted in a lower pressure distortion just upstream of the seal. A comparison of the endwall pressure distributions upstream of the baseline and modified seals is shown in Figure 3. Pressure coefficient data from both seals at x/Cax = 1.22 are similar. The data from the modified seal was slightly higher than those from the baseline seal. Due to constraints on the instrumentation, pressure coefficient data were not available just upstream of the modified seal (at x/Cax = 1.30). A CFD prediction just upstream of the modified seal, however, indicates that the amplitude of the pressure variation was greatly reduced.

Increasing the overlap allowed the purge flow to exit the seal more uniformly. In the baseline seal shown in Figure 1c, little distance separated the point where the purge flow impinged on the underside of the vane endwall and the seal exit. Consequently, the purge flow egressed from the seal near the top of the exit as shown by Gibson et al. [24]. By extending the overlap, the purge flow had more distance to turn and exit more uniformly across the seal exit, thereby preventing ingress near the blade endwall more effectively.

Extending the vane endwall also decreased the trench width in the modified seal by 28% relative to the trench width in the baseline seal. A parametric study by Gibson et al. [1] showed the decrease in trench width led to improved sealing and endwall cooling. Decreasing the trench width reduces the area through which hot gas from the main gas path may enter into the trench resulting in higher sealing effectiveness and adiabatic effectiveness.

The present work illustrates the effect of the main gas path pressure field on the flowfield in an engine-relevant rim seal. By using a stationary seal, the impact of the main gas path pressure field on the seal flow is more clearly determined by removing the effects of rotation and unsteady effects in the main gas path. It is expected, however, that changes will occur to the seal flowfield once rotational effects rea included. Disk pumping has been observed to increase the momentum deep inside the seal while the rotation of the blade endwall will, through viscous interaction; increase the tangential velocity component in the seal [3]. Additionally, unsteady interactions in the main gas path will disrupt the flowfield in the seal causing hot gas to be introduced into the seal. The trends reported here provide context for understanding the rotating flowfield by providing a comparison to the flowfield present in the seal when only pressure effects act upon it.

EFFECTS OF VANE GEOMETRY

Hot gas ingress beneath the platform has been observed to be influenced by the pitchwise pressure variation, or distortion, imposed on the rim seal by an upstream airfoil row [7]. To study the sensitivity of the rim seal to the pressure distortion of an upstream vane row, the geometry of the vane was altered to reduce the pressure distortion over the seal. The main geometric parameters, listed in Table 1, of the altered vanes, referred hereafter as the low-distortion vanes, match those of the baseline vane. Local changes were made to the vane curvature distributions such that static pressure distortion above the rim cavity was altered while maintaining other vane exit conditions such as wake deficit and flow angles. Modifying the vane did result, however, in a slightly different turning angle for the low-distortion vanes and the baseline vanes, 71° and 72° respectively. Periodicity was observed in the mid-span pressure distributions for the low-distortion vanes as shown in [1].

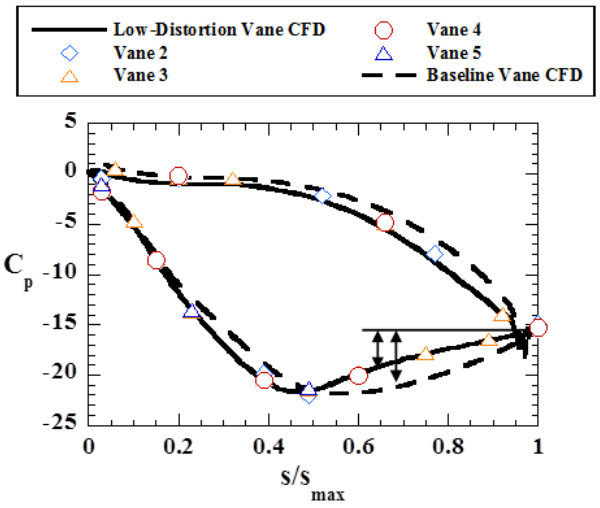

Figure 4. Mid-span pressure distribution around the low-distortion vanes.

The distortion imposed by a vane row on a downstream rim seal is characterized by the difference between the high-pressure region behind the trailing edge and the low-pressure region on the suction side of the vane, as illustrated by the arrows in Figure 4. Comparing the pressure distributions in Figure 4 illustrates the differences in the pressure distortions imposed on the rim seal by the two sets of vanes. The pressure distribution on the suction side of the low-distortion vane increases more rapidly downstream of the throat than that on the baseline vane. As a result, the downstream rim seal was exposed to a more uniform pressure field and therefore experiences less distortion compared to when the baseline vanes are present.

Average sealing effectiveness for the baseline vanes and the low-distortion vanes is compared in Figure 5. Average sealing effectiveness shows no appreciable change between the baseline and low-distortion vanes. The insensitivity of the average sealing effectiveness in Figure 5 indicates that the pressure distortion of the baseline vane was not the dominant driver of hot gas ingress for this experiment. Such insensitivity of the rim seal to the upstream pressure distortion is somewhat surprising given the results of previous studies [5-7]. One possible explanation for this insensitivity may be the ability of the radial overlap seal to minimize the effect of the main gas path pressure field on the seal exit. The seal exit is separated from the main gas path by the flow in the trench. The insensitivity of the seal flow to the main gas path pressure field is supported by Gibson et al. [24], who report that circumferential pressure variations from the vane row had little effect on the trench flowfield.

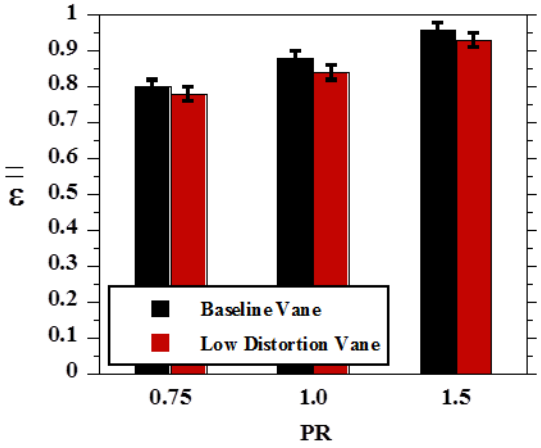

Figure 5. Comparison of sealing effectiveness for the baseline and low-distortion vanes.

EFFECTS OF DOWNSTREAM BLUFF BODIES

The effect of the downstream bluff bodies (simulating the downstream blades) on sealing was determined. Average sealing effectiveness and adiabatic effectiveness levels, for the purge flow ratio of 0.75%, were measured with the bluff bodies present and without them. As shown in Figure 6, placing the bluff bodies downstream of the trench reduced the cooling in the trench region as demonstrated by reduced adiabatic effectiveness levels. Contours of adiabatic effectiveness in Figure 7 show that the bluff bodies decreased adiabatic effectiveness throughout the trench. The decrease was observed especially in the downstream portion of the trench ($x/C_{ax} \approx 0.30$), just upstream of the bluff bodies, due to hot gas from the mainstream entering the trench. Additionally, the bluff bodies did not change the pressure distribution upstream of the seal; confirming that their effects were strongest in the back of the trench. Hot gas entering the trench not only reduced adiabatic effectiveness, but also sealing effectiveness as shown in Figure 6. The bluff bodies therefore not only drove more hot gas into the trench region, but also caused increased amounts of hot gas to enter the seal exit which reduced sealing effectiveness.

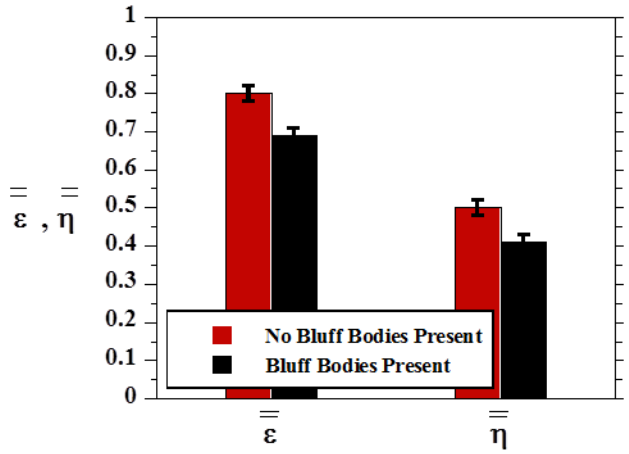

Figure 6. The effect of bluff bodies on average sealing and adiabatic effectiveness (PR = 0.75%).

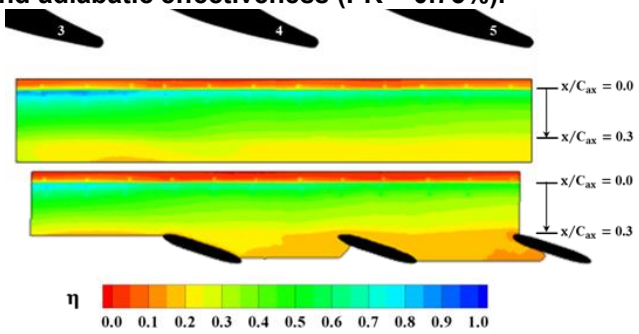

Figure 7. Contours of adiabatic endwall effectiveness in the trench with and without the bluff bodies present (PR = 0.75%).

To identify how the external pressure field downstream of the seal affects the sealing and endwall temperature, the mean flowfields with and without the bluff body airfoils present are compared. As described previously, flowfield measurements from two planes are presented here. One plane is located at mid-pitch between vanes 3 and 4 (y/P= 0.6) and is shown in Figures 8a-b. The other, which is shown in Figures 9a-b, is located behind the trailing edge of vane 4 (y/P= 1.1). Contours showing tangential velocity, defined as V in Figure 1a, normalized by the cascade inlet velocity (U_i) are overlaid with vectors representing the in-plane motion of the flow as determined by the axial and spanwise velocities, which are defined as U and W respectively in Figures 1a-b.

At mid-pitch, shown in Figure 8a, the flow above the trench was characterized by a mixing layer which transitioned from the low-velocity purge flow in the trench to the higher velocity flow in the mainstream. Placing the bluff bodies downstream of the trench did not qualitatively change the flowfield at mid-pitch; hence the contours in Figures 8a-b showed very similar patterns.

In contrast to their negligible effects at mid-pitch, the bluff bodies had a more prominent impact on the vane trailing edge plane. Without the bluff bodies, as shown in Figure 9a, the most prominent feature of the flowfield behind the vane trailing edge

was the vane passage vortex entraining low-velocity purge flow from the trench into the mainstream, as explained by Gibson [24]. The presence of the bluff bodies further complicated this region of the flowfield by causing the mainstream flow to stagnate near the leading edge of the bluff body, as shown in Figure 9b. Flow stagnation was evident by the decreased tangential velocity on the downstream side of the trench at the vane trailing edge plane (Figure 9b). The proximity of the leading edge of the middle bluff body to this region was shown in Figure 1a.

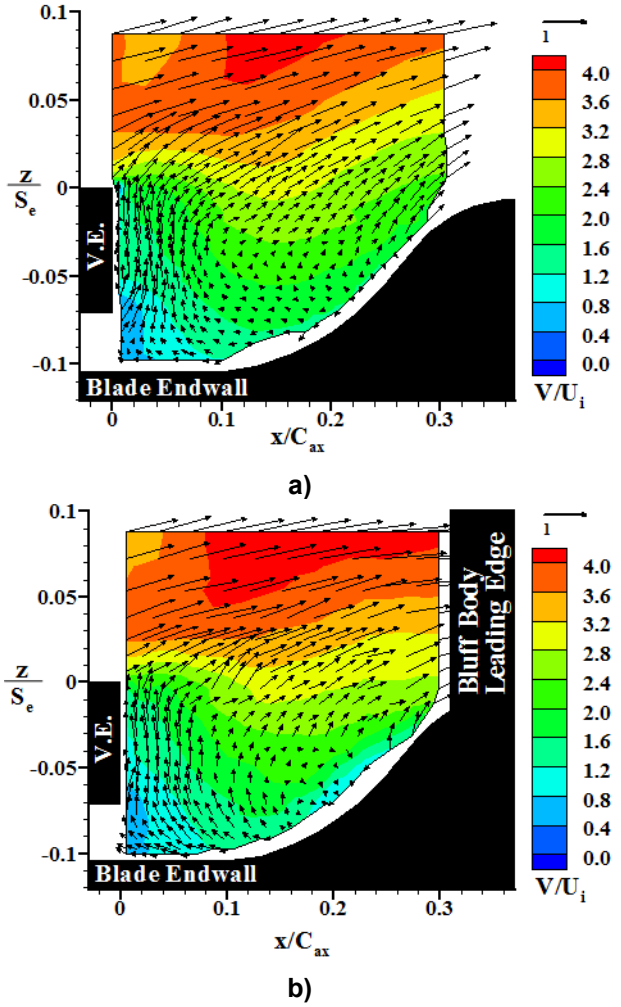

Figure 8. Normalized mean tangential velocity with in-plane vectors for the mid-pitch plane (y/P = 0.6) a) without and b) with bluff bodies (PR = 0.75%).

Flow stagnation on the bluff body resulted in a region of high static pressure above the trench. Consequently, flow entering these regions of high pressure was deflected from the main gas path into the trench, resulting in the small recirculation zone observed in the mean vectors in Figure 9b and illustrated by the white arrow. The flowfield measurements by Gallier et al. [9] also showed that the secondary flows of a downstream blade affected an upstream seal. The size of the secondary flow structures varied as the rotating blade interacted with the pressure field of the upstream vane. It is quite possible that the size and intensity of the recirculation zone in Figure 9b would also become highly unsteady were rotation included in the experiment. By deflecting hot gas into the trench, the bluff bodies decreased the adiabatic effectiveness levels in the downstream portion of the trench as shown in the contours of Figure 7. The bluff bodies were designed to match the pressure distortion of a downstream blade, but not the endwall flows of a blade. Given the large leading edge of a blade relative to that of the bluff bodies, it is reasonable that a blade would deflect a greater amount of hot gas into the trench in its horse shoe vortex and further reduce adiabatic effectiveness.

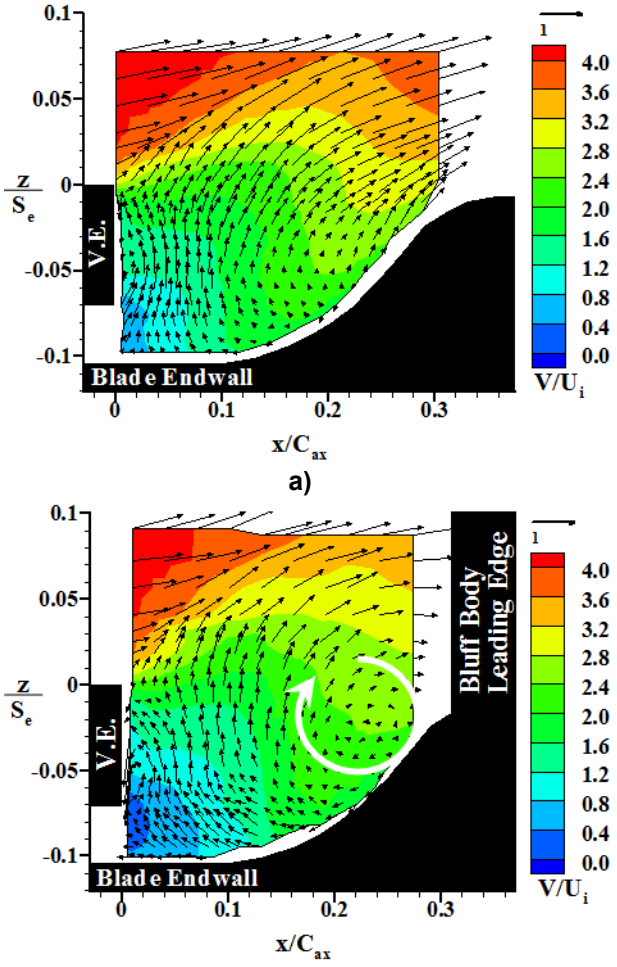

Figure 9. Normalized mean tangential velocity with in-plane vectors for the vane trailing edge plane (y/P = 1.1) a) without and b) with bluff bodies (PR = 0.75%).

As the hot gas deflected by the bluff bodies enters the trench, it causes a change in the flow angle near the seal exit. To quantify the impact of the bluff bodies, profiles of flow angle (defined as yaw angle in the nomenclature section) from just downstream of the vane endwall (x/C_{ax}= 0.02) are shown in Figure 10. For a spanwise position of $-0.1 \leq z/S_e \leq -0.07$, these profiles describe the flow just outside the seal exit. For

reference, the spanwise location of the seal exit is also marked on Figure 10. A yaw angle of less than 90° just outside of the seal exit denotes flow that is exiting the seal (also called egress), whereas a yaw angle greater than 90° indicates flow ingress (flow that is entering the seal).

Without the bluff bodies present, the mean flow in front of the seal exit showed slight egress with the average yaw angle ranging from 76° near the top of the seal exit and 90° near the bottom, as shown in Figure 10. Hot gas deflected by the bluff bodies into the back of the trench, however, increased the yaw angle by turning the flow in the upstream portion of the trench towards the seal exit. Higher yaw angles denoted that more mean flow entered the seal exit, decreasing the sealing effectiveness as shown in Figure 6. The effect of the bluff bodies on the average yaw angle was greater behind the vane trailing edge due to the proximity of that plane to the leading edge of the middle bluff body. Yaw angle was also consistently higher near the bottom of the seal exit (z/S_e = -0.1) than at the top (z/S_e = -0.07) indicating that hot gas ingress was more likely to happen near the blade endwall than at the top of the seal exit where the bulk of the purge flow egress occurred.

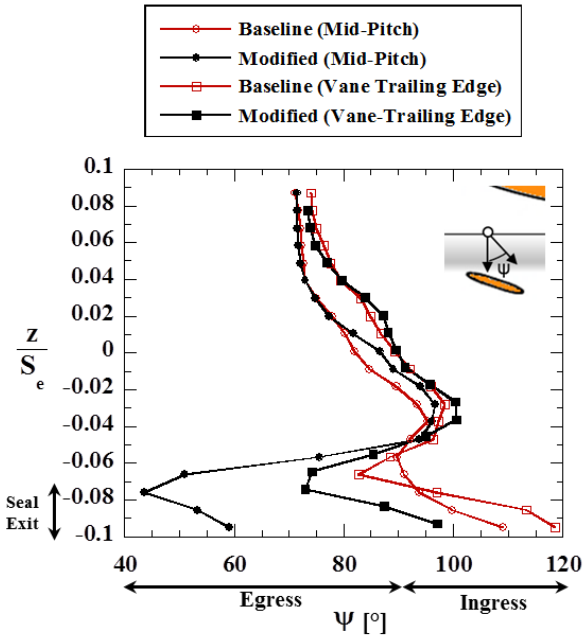

Figure 10. Profiles of average flow angle downstream of the seal exit, x/C_{ax}= 0.02 (PR = 0.75%).

Contours of turbulence intensity (defined as Tu in the nomenclature section) with and without the bluff bodies present at the vane trailing edge plane are given in Figures 11a-b. First, it is quite apparent that these are very high turbulence levels (0.35 – 2.0), which explains the pitchwise uniformity of the adiabatic effectiveness measurements in Figure 7. Evidence of high turbulent mixing has also been observed in the rim seal of a high-speed turbine rig. The sealing effectiveness measurements made by Clark et al. [25] show that coolant rapidly dissipated in the rim seal leading to diminished sealing.

The unsteady or turbulent behavior near the exit of the seal has been attributed in the literature to the unsteady interactions between adjoining airfoil rows [5,9]. The steady nature of the present work eliminates such unsteady interactions. A key contribution of this work is the high turbulence intensity levels presented here which indicate that unsteadiness in the seal flowfield is also driven by the interaction between the purge flow exiting the seal and the separated flow behind the vane endwall.

Adding the bluff bodies increased the peak turbulence intensity at the seal exit from 0.7 in Figure 11a to 2.0 in Figure 11b. The large increase in Tu was primarily driven by a decrease in local velocity magnitude at the seal exit (shown in Figures 9a and 9b). The turbulence intensity at mid-pitch was insensitive to the presence of the bluff bodies and so will not be presented. Given the insensitivity of the turbulence at mid-pitch to the bluff bodies, the increase in turbulence intensity behind the vane trailing edge was likely due to the hot gas deflected into the trench by the bluff bodies.

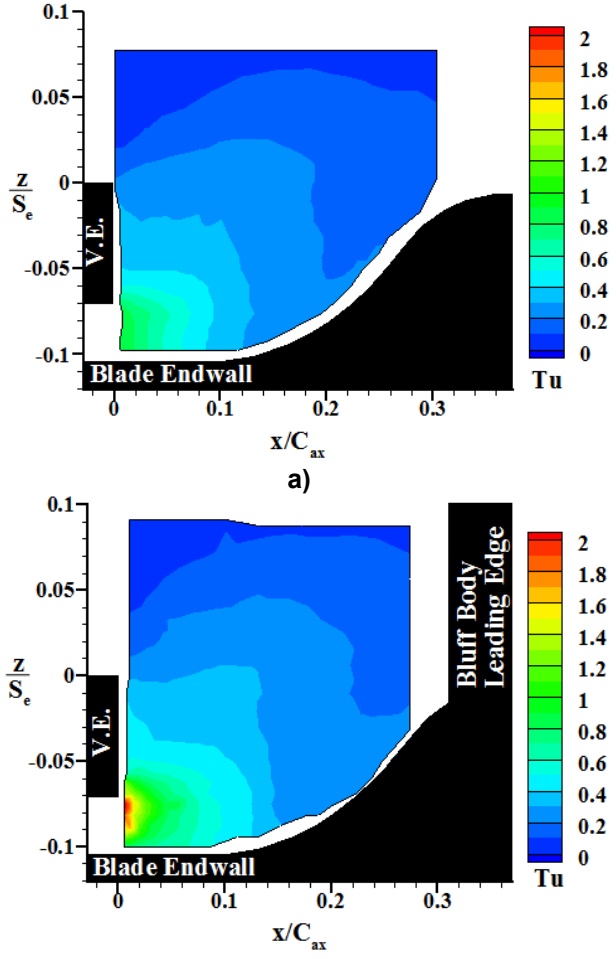

Figure 11. Contours of turbulence intensity for the vane trailing edge plane (y/P = 1.1) a) without and b) with bluff bodies (PR = 0.75%).

Changes in the trench flow due to the bluff bodies also affected flow structures associated with aerodynamic losses. Mainstream flow stagnating on the bluff bodies enlarged the region of low-velocity flow already present in the main gas path, increasing the potential for mixing losses to occur. The bluff bodies, however, also potentially reduced losses by thinning the boundary layer on the blade endwall especially at mid-pitch. Comparison of the contours of V/U_i at the mid-pitch plane without the bluff bodies (Figure 8a) and with bluff bodies (Figure 8b) showed a decrease in the boundary layer height at the back of the trench indicating flow was accelerated around the bluff bodies. Schuler et al. [11] noted thickening the boundary with low-velocity purge flow created more aerodynamic losses

EFFECT OF RIM SEAL GEOMETRY

Improvements in rim seal design are often focused on enhancing the ability of a seal to prevent the ingress of hot gas into the spaces beneath the endwall and increasing the cooling of the downstream endwall. Increasing the axial overlap showed improvements in both of these objectives. The increases in both sealing effectiveness and adiabatic effectiveness, shown in Figure 12, associated with the modified seal indicate that increasing the axial overlap improves seal performance. In design, manufacturing and geometric tolerances often constrain how much axial overlap is possible in the seal. The sealing effectiveness data and the accompanying flowfield measurements, however, may provide insight into the performance trends in the design space that exists in the engine.

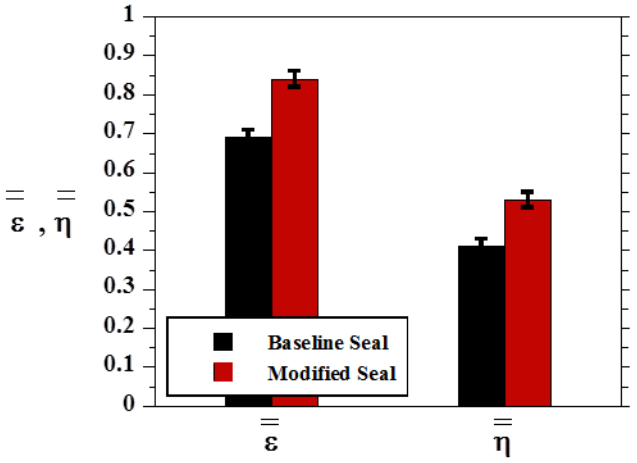

Figure 12. The effect of rim seal geometry on average sealing and adiabatic effectiveness (PR=0.75%).

The mean flowfields in the baseline and modified seals were compared in Figures 13a-b and 14a-b to explain how increasing the axial overlap improved sealing and endwall cooling. Endwall cooling in the baseline seal was reduced because purge flow leaving the seal exit was immediately turned away from the blade endwall, as demonstrated in Figures 13a and 14a. Gibson et al. [24] showed that the purge flow was simultaneously being pulled upward by the vane passage vortex and entrained by the high-velocity flow in the trench. In the modified seal, however, the purge flow traveled laterally along the blade endwall, cooling that surface more effectively than in the case with the baseline seal. The recirculation zone near the bluff body leading edge in Figure 14b, however, limited how far along the blade endwall the purge flow could travel at the vane trailing edge plane. Since the modified seal allowed the purge flow to remain close to the blade endwall, the blade endwall was better cooled resulting in the improved adiabatic effectiveness reported in Figure 12.

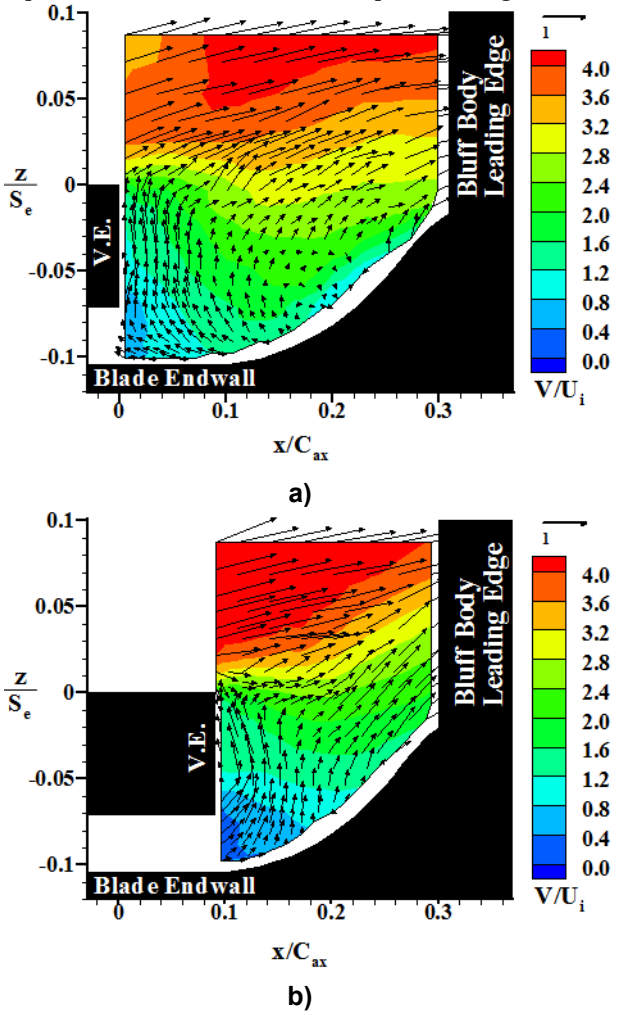

Figure 13. Contours of normalized tangential velocity with in-plane vectors from the mid-pitch plane (y/P = 0.6) a) without and b) with bluff bodies (PR = 0.75%).

Purge flow was able to remain close to the blade endwall and fill more of the trench for the modified seal design. One reason for this was that the high velocity that was previously mentioned to entrain the purge flow was reduced in the modified seal. The contours of normalized tangential velocity (V/U_i) at both planes in the baseline seal (Figures 13a and 14a) show that the levels of V/U_i in the back of the trench (x/C_{ax} > 0.15) are many times higher than the levels of V/U_i at the seal

exit. The contours from the modified seal (Figures 13b and 14b), however, showed that the V/U_i levels in the downstream portion of the trench (x/C_{ax} > 0.15) were much more similar to the seal exit levels than in the baseline seal.

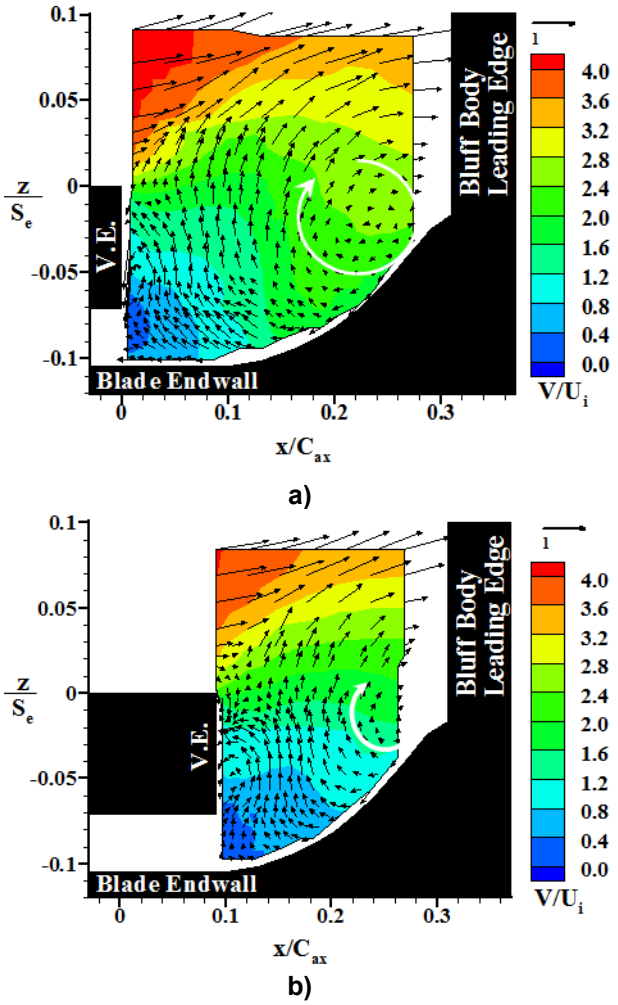

Figure 14. Contours of normalized tangential velocity with in-plane vectors from the vane trailing edge plane (y/P = 1.1) a) without and b) with bluff bodies (PR = 0.75%).

The improved sealing effectiveness in the modified seal was the result of the purge flow remaining closer to the blade endwall. Purge flow exited the baseline seal near the top of the seal exit as demonstrated by the vectors in Figures 13a and 14a. As can be seen in Figure 1c, a short distance separated the hairpin turn in the baseline seal and the seal exit. As a result, the purge flow impinged on the underside of the vane endwall and exited near the top of the seal exit. While the purge flow exited at the top of the seal, the mean vectors in Figure 13b show that hot gas from the trench was able to enter the seal along the blade endwall. In contrast, the modified seal increased the axial distance between the final turn in the seal and the seal exit. Therefore, the purge flow had more distance to fully develop and exit more uniformly across the span of the seal exit, as shown by the vectors in Figure 14b.

The increased penetration of purge flow into the modified trench caused a profound change in the flow angle, shown in Figure 15. Profiles from both seals are shown for the upstream portion of the trench (x/C_{ax} = 0.024 and 0.10 in the baseline and modified seals respectively). The flow just outside the seal exit is represented by the profiles in the upstream portion of the trench between spanwise locations of $-0.1 \le z/S_e \le -0.07$. Near the seal exit, the yaw angle for both planes was lower in the modified seal. Yaw angles in the baseline seal indicated moderate ingress levels ($\psi \approx 110°$). In contrast, the yaw angle in front of the seal exit indicated strong egress of purge flow from the seal ($\psi \approx 60°$). Egress was more pronounced at mid-pitch than behind the vane trailing edge due to the dominance of the recirculation zone below the bluff body leading edge, shown in Figures 14a-b, at the vane trailing edge plane. The strong egress in the modified seal supports the enhanced sealing effectiveness shown in Figure 12.

While the modified seal decreased the amount of hot gas entering the seal; it also increased the scale of flow structures which are associated with aerodynamic losses. Inspection of the contours of normalized tangential velocity in Figures 13b and 14b indicate that the boundary layer on the downstream endwall was thicker in the modified seal. Thickening the boundary layer, as previously discussed, leads to higher aerodynamic losses.

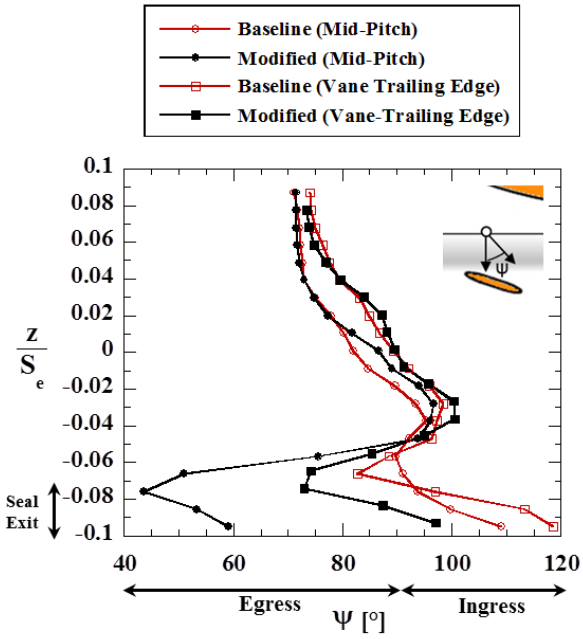

Figure 15. Profiles of average flow angle from the upstream portion of the trench (x/C_{ax} = 0.024 and 0.10 in the baseline and modified seals respectively) for PR = 0.75%.

Contours of turbulence intensity from the trailing edge plane (y/P=1.1) for the baseline and modified seal, shown in Figures 16a-b, illustrate the impact of seal modification on the turbulence in the trench. A significant reduction in peak turbulence levels is observed at the seal exit. Turbulence levels

dropped from 2.0 in the baseline seal to approximately 1.0 in the modified seal. Despite the decrease in peak levels, the turbulence intensity at the seal exit remained of the order of magnitude as the local velocity vector. The turbulence levels at mid-pitch (y/P = 0.6) followed the same trends as those at the vane trailing edge plane and so will not be shown here.

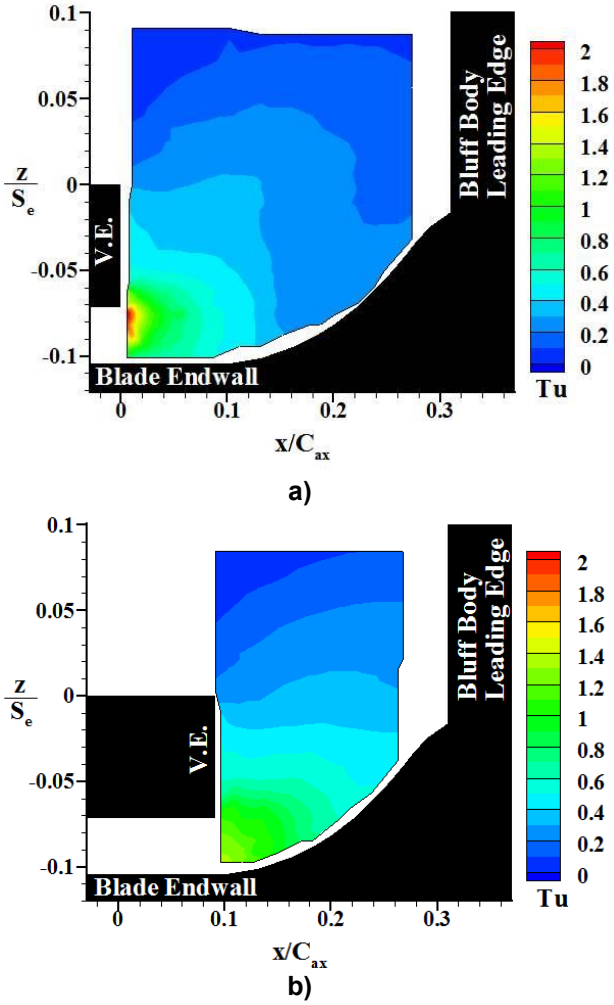

Figure 16. Contours of turbulence intensity for the vane trailing edge plane (y/P = 1.1) a) in the baseline seal and b) the modified seal (PR = 0.75%).

Increasing the axial overlap also had a significant impact on the turbulence levels in the back of the trench. Comparing the contours from the baseline seal Figure 16a) to those from the modified seal (Figure 16b), turbulence intensity levels increased in the back of the trench from 0.3 to approximately 0.8. The modified seal increased the mixing of the purge flow and the hot gas from the mainstream, leading to the minimal gradients in adiabatic effectiveness in the trench.

Previous investigations attribute the highly unsteady flow in the seal to the unsteady interactions between adjoining airfoil rows [5, 9]. From this point of view, a seal designer may try to increase seal overlap to isolate the seal from the unsteady flow in the main gas path. The high levels of turbulence intensity in the baseline seal, however, indicate that unsteady effects are not the only driver of unsteadiness in the seal. Furthermore, the high turbulence intensity levels in the modified seal show that increasing axial overlap may not decrease unsteadiness in the seal flow.

CONCLUSIONS

The impact of the main gas path pressure field and seal geometry on the flowfield in the trench of an engine-relevant rim seal was studied using a large-scale, linear cascade. Bluff bodies were designed to match the pressure distortion of a rotating blade downstream of the seal. Adding the bluff bodies downstream of the seal increased the amount of hot gas in the trench and seal, demonstrated by a decrease in sealing effectiveness and adiabatic endwall effectiveness. Flowfield measurements showed that mainstream flow was deflected by the bluff bodies into the downstream portion of the trench, decreasing the adiabatic effectiveness in that area. The deflected flow from the bluff bodies altered the mean flow angle causing more flow ingress into the seal reducing the sealing effectiveness.

The sensitivity of the rim seal to the pressure distortion of an upstream vane row was also studied. Through modifying the vane geometry, the pressure distortion imposed on the rim seal by the vane was reduced. Despite the reduced circumferential pressure distortion, however, no significant change in sealing effectiveness was observed. It was noted therefore that the ability of the pressure distortion of the upstream vane row to drive hot gas ingress could be geometry specific.

Increasing the axial overlap at the seal exit improved sealing effectiveness and adiabatic effectiveness. Extending the vane endwall decreased the influence of the passage vortex on the purge flow and reduced the velocity in the trench. As a result, the purge flow reached farther into the trench before mixing with the hot gas from the main gas path, increasing the sealing effectiveness and adiabatic effectiveness.

High levels of turbulence intensity were measured in both the baseline and modified seals. Historically, high levels of unsteadiness in the seal have been attributed to unsteady interactions between neighboring airfoil rows in the main gas path. Since the present work eliminated such unsteady effects, it is evident that unsteadiness in the seal flow is also due to the interaction between the purge flow and the separated flow in the trench region of the seal. Increasing the axial overlap did not reduce turbulence intensity, suggesting that eliminating unsteadiness in the seal through geometry changes may be difficult.

The flowfield measurements presented in the current work also impact modeling efforts to predict seal behavior. The present experiments did not include rotational or unsteady main gas path effects. As a result, CFD models can be compared against the flowfields presented by the authors to ascertain how well the models capture the seal flowfield without the further complication of rotation.

ACKNOWLEDGMENTS

The authors would like to acknowledge the support of the NASA fixed wing NRA program. Contract number: NNC11TA41T. This document has been publically released.

REFERENCES

[1] Gibson, J., Thole, K.,Christophel, J., Memory, C., 2015, "Effects of the Main Gas Path Pressure Field on Rim Seal Flows in a Stationary Linear Cascade", *Proceedings of ASME Turbo Expo* 2015, GT2015-43517.

[2] Johnson, B.V., Mack, G.J., Paolillo, R.E., Daniels, W.A., 1994, "Turbine Rim Seal Gas Path Flow Ingestion Mechanisms" *30th AIAA/ASME/SAE/ASEE Joint Propulsion Conference*, AIAA94-2703.

[3] Phadke, U.P., Owen, J.M., 1988, "Aerodynamic Aspects of *the* Sealing of Gas-Turbine Rotor-Stator Systems Part 2: The Performance of Simple Seals in a Quasiaxisymmetric External Flow" *International Journal of Heat and Fluid Flow*, **9**(2).

[4] Johnson, B.V., Jakoby, R., Bohn, D.E., Cunat, D., 2009, "A Method for Estimating the Influence of Time-Dependent Vane and Blade Pressure Fields on Turbine Rim Seal Ingestion" *JTurboMach* **131**(2). doi: 10.1115/1.2950053

[5] Roy R. P., Feng J., Narzary D., Saurabh P., Paolillo R.E., 2005, "Experiments on Gas Ingestion Through Axial-Flow Turbine Rim Seals", *J.TurboMach*., **127**(3). doi: 10.1115/1.1850499.

[6] Wang, C.-Z., Cloud, D., Paolillo, R., Vashist, T.K., Johnson, B.V., Roy, R.P., 2006, "Rim Seal Ingestion Characteristics for Axial Gap Rim Seals in a Closely-Spaced Turbine Stage from a Numerical Simulation" *Proceedings of ASME Turbo Expo* 2006, GT2006-90965.

[7] Green T., Turner A.B., 1994, "Ingestion into the Upstream Wheel-space of an Axial Turbine Stage" *J. Turbomach*, **116**(2). doi:10.1115/1.2928368

[8] Bohn D., Rudzinski B., Surken N., Gartner W., 2000, "Experimental and Numerical Investigation of the Influence of Rotor Blades on Hot Gas Ingestion into the Upstream Cavity of an Axial Turbine Stage" *Proceedings of ASME Turbo Expo 2000*, ASME Paper No. 2000-GT-284.

[9] Gallier K.D., Lawless P.B., Fleeter S., 2004, "Development of the Unsteady Flow on a Turbine Rotor Platform Downstream of a Rim Seal" *Procceedings of ASME Turbo Expo 2004*, GT2004-53899. doi: 10.1115/GT2004-53899

[10] Jenny, P., Abhari, R.S., Rose, M.G., Brettschneider, M., Engel, K., Gier, J., 2013, "Unsteady Rotor Hub Passage Vortex Behavior in the Presence of Purge Flow in an Axial Low Pressure Turbine," *J.Turbomach*, **135**(5). doi: 10.1115/1.4007837

[11] Schuler, P., Kurz, W., Dullenkopf, K., Bauer, H.-J., 2010, "The Influence of Different Rim Seal Geometries on Hot-Gas Ingestion and Total Pressure Loss in a Low-Pressure Turbine" *Proceedings of ASME Turbo Expo 2010*, GT2010-22205.

[12] De la Rosa Blanco, E., Hodson, H., Vazquez, R., 2009, "Effect of the Leakage Flows and the Upstream Platform Geometry on the Endwall Flows of a Turbine Cascade" *J.TurboMach.*, **131**(1). doi:10.1115/1.2950052.

[13] McLean, C., Camci, C., Glezer, B., 2001, "Mainstream Aerodynamic Effects Due to Wheelspace Coolant Injection in a High-Pressure Turbine Stage: Part II: Aerodynamic Measurements in the Rotational Frame" *J.TurboMach*., **123**(4). doi: 10.1115/1.1397303.

[14] McLean, C., Camci, C., Glezer, B., 2001, "Mainstream Aerodynamic Effects Due to Wheelspace Coolant Injection in a High-Pressure Turbine Stage: Part II: Aerodynamic Measurements in the Stationary Frame" *J.TurboMach*., **123**(4). doi: 10.1115/1.1401026.

[15] Rehder, H-J, Dannhauer, A., 2007, "Experimental Investigation of Turbine Leakage Flows on the Three-Dimensional Flow Field and Endwall Heat Transfer" *J.TurboMach*., **129**(3). doi: 10.1115/1.2720484

[16] Abe T., Kikuchi J., Takeuchi H., 1979, "An Investigation of Turbine Disk Cooling (Experimental Investigation and Observation of Hot Gas Flow into a Wheel Space)" *13th International Congress on Combustion Engines (CIMAC)*.

[17] Mirzamoghadam A., Giebert D., Molla-Hosseini K., Bedrosyn L., 2012, "The Influence of HPT Forward Disc Cavity Platform Axial Overlap Geometry on Mainstream Ingestion" *Proceedings of ASME Turbo Expo 2012*, GT2012-68429.

[18] Paniagua, G., Denos, R., Almeida, S., 2004 "Effect of the Hub Endwall cavity Flow on the Flow-Field of a Transonic High-Pressure Turbine," *J. Turbomach*, **126**(4). doi: 10.1115/1.1791644

[19] Popovic I. and Hodson H.P., 2012, "Improving Turbine Stage Efficiency and Sealing Effectiveness Through Modifications of the Rim Seal Geometry" *J.TurboMach*., **135**(6). doi: 10.1115/1.4024872.

[20] Marini, R., Girgis, S., 2007, "The Effect of Blade Leading Edge Platform Shape on Upstream Disk Cavity to Mainstream Flow Interaction of a High-Pressure Turbine Stage", *Proceedings of ASME Turbo Expo* 2007, GT2007-27429. doi: 10.1115

[21] Lynch, S., Sundaram, N., Thole, K., Kohli, A., Lehane, C., 2011, "Heat Transfer for a Turbine Blade with Nonaxissymmetric Endwall Contouring," *JTurboMach.*, **133**(1). doi: 10.1115/1.4000542

[22] Moffat, R.J., 1985, "Using Uncertainty Analysis in the Planning of an Experiment" *J Fluids Engineering*, **107**(2). doi:10.1115/1.3242452

[23] Memory C., 2014, Engineer at Pratt and Whitney, private communication

[24] Gibson, J., "Geometric Effects on Static Turbine Rim Seals", PhD thesis, Department of Mechanical and Nuclear Engineering, The Pennsylvania State University.

[25] Clark, K., Barringer, M., Coward, A., Thole, K., Clum, C., Hiester, P., Memory, C., Robak, C., 2015. "Using a Tracer Gas to Quantify Sealing Effectiveness for Engine Realistic Rim Seals", *Proceedings of ASME Turbo Expo 2016*, GT2016-58095.